Adsorption of GST-PI3Kγ at the Air-Buffer Interface and at Substrate and Nonsubstrate Phospholipid Monolayers

ARTICLE *in* BIOPHYSICAL JOURNAL · MARCH 2009

Impact Factor: 3.97 · DOI: 10.1016/j.bpj.2008.10.032 · Source: PubMed

5 AUTHORS, INCLUDING:

Gerald Reiter
Max Planck Institute of Colloids and Interfaces
18 PUBLICATIONS **298** CITATIONS

SEE PROFILE

Adsorption of GST-PI3Kγ at the Air-Buffer Interface and at Substrate and Nonsubstrate Phospholipid Monolayers

Antje Hermelink,[†] Cornelia Kirsch,[‡] Reinhard Klinger,[‡] Gerald Reiter,[†] and Gerald Brezesinski[†*]
[†]Interface Department, Max Planck Institute of Colloids and Interfaces, Potsdam, Germany; and [‡]Medical Department, Institute of Biochemistry II, Friedrich Schiller University, Jena, Germany

ABSTRACT The recruitment of phosphoinositide 3-kinase γ (PI3Kγ) to the cell membrane is a crucial requirement for the initiation of inflammation cascades by second-messenger production. In addition to identifying other regulation pathways, it has been found that PI3Kγ is able to bind phospholipids directly. In this study, the adsorption behavior of glutathione *S*-transferase (GST)-PI3Kγ to nonsubstrate model phospholipids, as well as to commercially available substrate inositol phospholipids (phosphoinositides), was investigated by use of infrared reflection-absorption spectroscopy (IRRAS). The nonsubstrate phospholipid monolayers also yielded important information about structural requirements for protein adsorption. The enzyme did not interact with condensed zwitterionic or anionic monolayers; however, it could penetrate into uncompressed fluid monolayers. Compression to values above its equilibrium pressure led to a squeezing out and desorption of the protein. Protein affinity for the monolayer surface increased considerably when the lipid had an anionic headgroup and contained an arachidonoyl fatty acyl chain in *sn*-2 position. Similar results on a much higher level were observed with substrate phosphoinositides. No structural response of GST-PI3Kγ to lipid interaction was detected by IRRAS. On the other hand, protein adsorption caused a condensing effect in phosphoinositide monolayers. In addition, the protein reduced the charge density at the interface probably by shifting the pK values of the phosphate groups attached to the inositol headgroups. Because of their strongly polar headgroups, an interaction of the inositides with the water molecules of the subphase can be expected. This interaction is disturbed by protein adsorption, causing the ionization state of the phosphates to change.

INTRODUCTION

Phosphatidylinositol and its phosphorylated derivatives play crucial roles in a broad range of signal transduction processes. Phosphoinositide 3-kinase γ (PI3Kγ) belongs to the class of phosphoinositide kinases phosphorylating the 3-position of the inositol ring of phosphatidylinositols, which have been shown to be involved in numerous cellular processes such as chemotaxis, cell proliferation, phagocytosis, and platelet aggregation (1–7). This enzyme is primarily activated by the $\beta\gamma$ subunits of heterotrimeric G-proteins (8) and is involved in signal transduction events linked to G-protein-coupled receptors (9,10). The physiologic relevance of PI3Kγ is not restricted to its lipid kinase activity. An additional protein kinase function was also identified (11). The protein is able to interact with βARK1, thereby regulating β-adrenergic receptor signaling in cardiomyocytes (12), and, by interacting with PDE3B, PI3Kγ indirectly hydrolyzes cAMP in cardiac cells (13). The ability of PI3Kγ to associate with anionic phospholipids allows the kinase to be membrane resident without interacting with other protein components, which has been demonstrated for the immobilized form of the protein (14). This PI3Kγ isoform was originally cloned from hematopoetic cells, and it regulates thymocyte development, T-cell activation, neutrophil migration, and the oxidative burst (15,16). PI3Kγ associates with a noncatalytic p101 or p84 protein that shows no homology with any known protein (8,17). Whereas expression data have suggested that PI3Kγ forms a trimeric complex (p110γ/p101/G$\beta\gamma$) at the plasma membrane (18), the mechanism of membrane binding is still unknown.

Determining structure/function relations for such proteins and lipids requires conditions that mimic the interfacial environment in which the molecules function. The thermodynamic relationship between monolayers and bilayers is direct (19). Monomolecular films at the air-water interface are membrane model systems that can be easily varied in terms of lipid composition, lipid lateral-packing density, surface pressure, and exposed area to the medium. The interaction of any protein with the membrane model interface is likely to change the lipid packing density and the lipid headgroup orientation and hydration. On the other hand, lipid structural properties can dictate the adsorption behavior of proteins by, e.g., inducing intramolecular structural responses.

Infrared reflection-absorption spectroscopy (IRRAS) is a powerful tool in the noninvasive study of molecular organization and interactions in and at Langmuir monolayers (20–23). Infrared absorptions are sensitive to the displacements of dipole moments, which depend on changes in conformation and chemical environment of functional groups involved in a normal mode of vibration. In recent years, IRRAS has become a standard technique to assess lipid conformation order and phase behavior. It is also an important and established method for molecular characterization of peptides and proteins (24) and is currently the only physical method that can directly monitor the secondary structure of proteins associated with Langmuir monolayers in situ (25).

Submitted May 5, 2008, and accepted for publication October 27, 2008.

*Correspondence: brezesinski@mpikg.mpg.de

Editor: Paul H. Axelsen.

0006-3495/09/02/1016/10 $2.00

doi: 10.1016/j.bpj.2008.10.032

The present work describes the adsorption of GST-PI3Kγ to the bare air-buffer interface as the simplest example of a hydrophobic–hydrophilic interface. IRRAS was used to draw conclusions about secondary structure elements present at this interface. Furthermore, the interactions of GST-PI3Kγ with substrate and nonsubstrate monolayers are discussed in detail. The influence of lipid charge (zwitterionic as well as anionic monolayers have been used) and of the monolayer phase state (involving disordered or ordered lipid layers) on the interaction with GST-PI3Kγ was investigated. The most prominent result is the finding that, besides an anionic headgroup, an arachidonoyl chain in *sn*-2 position is the crucial factor for strong adsorption. This indicates that the negative charge in the headgroup region and a special fatty-acid chain pattern are important for the regulation of signal transduction via PtdIns(3,4,5)P_3 and PI3Kγ. GST-PI3Kγ is able to bind substrate and nonsubstrate phospholipids, which demonstrates its multifunctionality. In cardiac contractility, PI3Kγ has distinct kinase-dependent and -independent functions, demonstrating its ability to act as a scaffold protein independent of its enzymatic activity (13).

MATERIALS AND METHODS

Materials

1,2-Dipalmitoyl-*sn*-glycero-3-phosphatidylinositol (DPPtdIns), 1,2-dipalmitoyl-*sn*-glycero-3-phosphatidylinositol-4,5-bisphosphate (DPPtdIns(4,5)P_2) (Cayman Chemicals, Ann Arbor, MI), 1,2-dioleoyl-*sn*-glycero-3-phosphatidylinositol (DOPtdIns), 1,2-dioleoyl-*sn*-glycero-3-phosphatidylinositol-4,5-bisphosphate (DOPtdIns(4,5)P_2), and 1-stearoyl-2-arachidonoyl-*sn*-glycero-3-phosphatylinositol-4,5-bisphosphate (SAPtdIns(4,5)P_2) (Avanti Polar Lipids, Alabama), as well as 1,2-distearoyl-*sn*-glycero-3-phosphatidic acid (DSPA), 1,2-distearoyl-*sn*-glycero-3-phosphocholine (DSPC), 1,2-dimyristoyl-*sn*-glycero-3-phosphocholine (DMPC), 1,2-dimyristoyl-*sn*-glycero-3-phosphatidic acid (DMPA), 1-stearoyl-2-arachidonoyl-*sn*-glycero-3-phosphatidic acid (SAPA), and 1-stearoyl-2-arachidonoyl-*sn*-glycero-3-phosphocholine (SAPC) (Sigma-Aldrich,Taufkirchen, Germany), were used as received. All the phosphatidylcholines were dissolved in chloroform, all the phosphatidic acids in chloroform:methanol (9:1, v/v), and the inositols in chloroform:methanol:water (65:35:6, v/v) (J.T. Baker, Deventer, Holland) to give 1 mM stock solutions. The aqueous subphase consisted of 10 mM Tris buffer, pH 8, 100 mM KCl, 10 mM NaCl, and 2 mM $CaCl_2$ (all from Sigma-Aldrich), referred to as Tris buffer throughout this article. For all subphases, Millipore (Billerica, MA) system purified water was used, giving a resistivity of 18.2 MΩcm.

Protein preparation

The recombinant GST-PI3Kγ was expressed in Sf9 cells. Isolation and purification of the GST-proteins used for the experiments have been described in former publications (11,14). The glutathione-4B-Sepharose-bound GST-PI3Kγ was eluted with buffer containing 50 mM Tris (pH 8.0) and 25 mM glutathione. The beads-free GST-PI3Kγ was dialyzed against 10 mM HEPES buffer (pH 7.2), 100 mM NaCl. The presence of 1% (w/w) Triton X-100 (Sigma-Aldrich) in the lysis buffer used for the preparation of the GST-fusion-proteins from Sf9 cells excluded the presence of significant amounts of contaminating lipids. As in many cases (26–28), the GST tag was not separated from the GST-fusion-protein. The attempt to remove the GST tag from the fusion proteins using thrombin or factor X_a led to yields too small to use in the preparation of sufficient amounts for the experiments described below.

Monolayer preparation

The monolayer experiments were performed on a film balance from R&K GmbH (Potsdam, Germany). The surface pressure was determined by the Wilhelmy method, using filter paper as Wilhelmy plate. The spread monolayer was allowed to equilibrate for 1 h. Symmetrical compression was achieved by means of two movable barriers at a velocity of 5 $Å^2$/(molecule per min). All experiments were performed at 20°C. The surfactant-free protein solution was injected either into the buffer solution or under a phospholipid monolayer equilibrated at 5 mN/m, leading to a final protein concentration of 0.5 μg/mL in the subphase. The incubation time was 30 min for monolayers containing substrates of the enzyme and 8 h for nonsubstrate phospholipid monolayers.

Infrared reflection-absorption spectroscopy (IRRAS)

Infrared reflection-absorption (IRRA) spectra have been recorded on an IFS 66 FT-IR spectrometer (Bruker, Germany) equipped with a liquid nitrogen-cooled mercury cadmium telluride detector. The infrared beam was conducted out of the spectrometer and focused onto the water surface of the thermostated Langmuir trough. If not otherwise indicated, the measurements were carried out with p-polarized light at one angle of incidence above (62°) and one below (40°) the Brewster angle. Measurements were performed using a trough with two compartments. One compartment contained the monolayer system under investigation (sample), whereas the other was filled with the pure subphase (reference). The trough was shuttled by a computer-controlled shuttle system to illuminate either the sample or the reference. The single-beam reflectance spectrum from the reference trough was taken as background for the single-beam reflectance spectrum of the monolayer in the sample trough to calculate the reflection-absorption spectrum as $-\log(R/R_0)$ to eliminate the water vapor signal. To maintain a constant water vapor content, the whole system was placed into a hermetically sealed box. Fourier transform infrared spectra were collected at 8 cm^{-1} resolution using 400 scans. IRRA spectra were simulated using software provided by Andreas Kerth (University of Halle, Germany).

RESULTS AND DISCUSSION

Adsorption of GST-PI3Kγ at the bare air-buffer interface

Adsorption of GST-PI3Kγ at the air-buffer interface was studied using surface pressure measurements and IRRAS. GST-PI3Kγ dissolved in Tris buffer displayed a pronounced surface activity. The surface pressure increased continuously during protein adsorption. Infrared bands related to the adsorbing protein appeared and grew, indicating an increasing protein concentration at the surface. The equilibrium surface pressure of the protein layer was reached after ~2 h and amounted to 9 mN/m. During the adsorption process, an IRRA spectrum was already taken at 5 mN/m (Fig. 1 *A, dashed line*). At 9 mN/m, the OH stretching band at ~3600 cm^{-1} was further increased (Fig. 1 *A, solid line*), compared to the spectrum at 5 mN/m, indicating an increase in the effective protein-layer thickness. The OH stretching band was reduced in the sample spectrum because of the replacement of the buffer by the adsorbed protein. As can be seen in

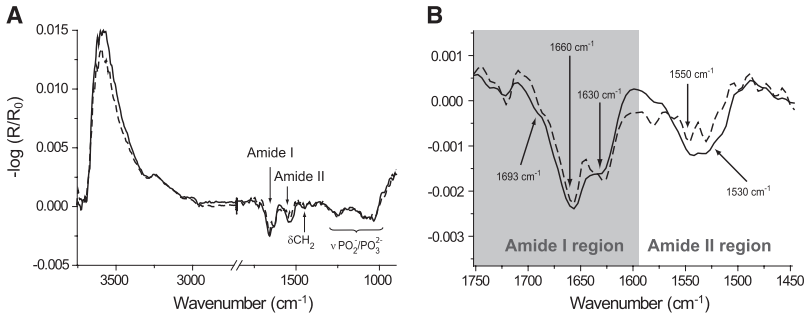

FIGURE 1 IRRA spectra of recombinant GST-PI3Kγ on Tris buffer acquired with p-polarized light at an angle of incidence of 40°. (*A*) GST-PI3Kγ at 5 mN/m (*dashed line*) and 9 mN/m (*solid line*). (*B*) Zoom-in into the amide region of the spectra presented in (*A*) with the same assignment of line types.

Fig. 1 *B (dashed* and *solid lines)*, the amide II band grew in a stronger intensity than the intensity of growth of the amide I band. This can be understood because the expected reflectance signal increase of amide I was partly compensated by the signal of the water bending band δ(OH) at ~1640 cm^{-1}. At 9 mN/m, the interface was saturated with protein. Compression of such a protein adsorption layer did not lead to any surface pressure increase, demonstrating that the protein cannot stay at the interface above that value and that it starts to desorb into the subphase.

Moreover, an additional intensity in the phosphate region between ~1000 cm^{-1} and ~1250 cm^{-1} was measured for the GST-PI3Kγ layer (Fig. 1 *A, dashed* and *solid lines*). This could be the result of posttranslational phosphorylation by autocatalysis or by other protein kinases. It should be noted that covalently attached carbohydrates also form intense broad bands at ~1100 cm^{-1}, because of the ν(CO) vibration of the sugar moieties, but no hint of glycosylation of the expressed kinase has yet been found.

The GST tag alone has only a weak surface activity (<2 mN/m), compared with that of the GST-PI3Kγ. This is qualitatively the same, as has been observed in the literature (29), but quantitatively different. Additionally, no IRRAS signals have been observed in experiments with lipid Langmuir monolayers. However, it should be noted that that the tag will contribute to the IRRA spectrum when attached to PI3Kγ, because it contains several α-helical and β-sheet secondary structure elements as well.

As depicted in Fig. 1 *B*, there are two bands in the amide I region with comparable intensity: one appearing as a shoulder at ~1630 cm^{-1}, indicating β-sheet secondary structure elements, and the other at 1660 cm^{-1}, indicating α-helical, random-coil, and/or β-turn secondary structure elements. It has already been shown that the C2 domain of PI3Kγ contains eight anti-parallel β-sheets and three turns (CBR1-3) (30). These turns are supposed to be responsible for the interaction with membranes. The band at 1660 cm^{-1} obtained in the GST-PI3Kγ IRRA spectra can be caused by either the turns (loops) of the C2 domain or structures of the GST tag. Amide II bands are rarely used for secondary structure determination. Nevertheless, the results match with those deduced from the amide I region, because the most intense contribution at ~1530 cm^{-1} indicated again the presence of β-sheet structures, whereas the band at ~1550 cm^{-1} could be attributed to α-helix elements of the GST tag.

To confirm this interpretation and to determine the orientation of the protein at the interface, IRRA spectra were measured at 9 mN/m with p-polarized light at incidence angles above (62°) and below (40°) the Brewster angle. The p-polarized light probes the dipole moment components parallel and perpendicular to the surface, and molecular orientations can be deduced. The amide I band is mainly associated with the C=O stretching vibration. The C-N stretching vibration and the N-H bending vibration are observable mainly in the amide II band region.

Fig. 2, *A–C* shows the amide region of GST-PI3Kγ spectra (*solid lines*) at the air-buffer interface at 9 mN/m. Simulated IRRA spectra (*dotted lines*) of α-helices (Fig. 2 *A*) and of antiparallel β-sheets (Fig. 2 *B*), both lying flat at the interface, and of random coils (Fig. 2 *C*), have been inserted for comparison (31). The simulation of β-sheets with different tilt angles revealed that the β-sheets of the GST-PI3Kγ are lying mainly flat at the interface. The broadening of the band in the region ~1550 cm^{-1} indicates a hindered orientation of the different β-sheets by the connecting turns (32). Moreover, the comparison of simulated and measured spectra also indicates considerable amounts of α-helical and random coil structures at the interface.

Adsorption of GST-PI3Kγ at nonsubstrate monolayers

To evaluate the adsorption properties of GST-PI3Kγ at phospholipid surfaces, different phospholipid monolayers were used to determine possible structural requirements for optimal adsorption. The lipid properties in focus were the packing density (phase state), different fatty-acid patterns, and the headgroup charge.

DSPC with a zwitterionic headgroup and two saturated fatty-acid chains forms exclusively condensed monolayer phases. DSPA has the same hydrophobic part, but it has an anionic headgroup. It, too, forms only condensed monolayer phases at all surface pressures. Independent of the headgroup charge, the protein is not able to interact with condensed phospholipid monolayers to the extent that it is detectable with IRRAS (Fig. 3 *A*). At 5 mN/m, the IRRA spectra are the same, irrespective of the presence of GST-PI3Kγ in the

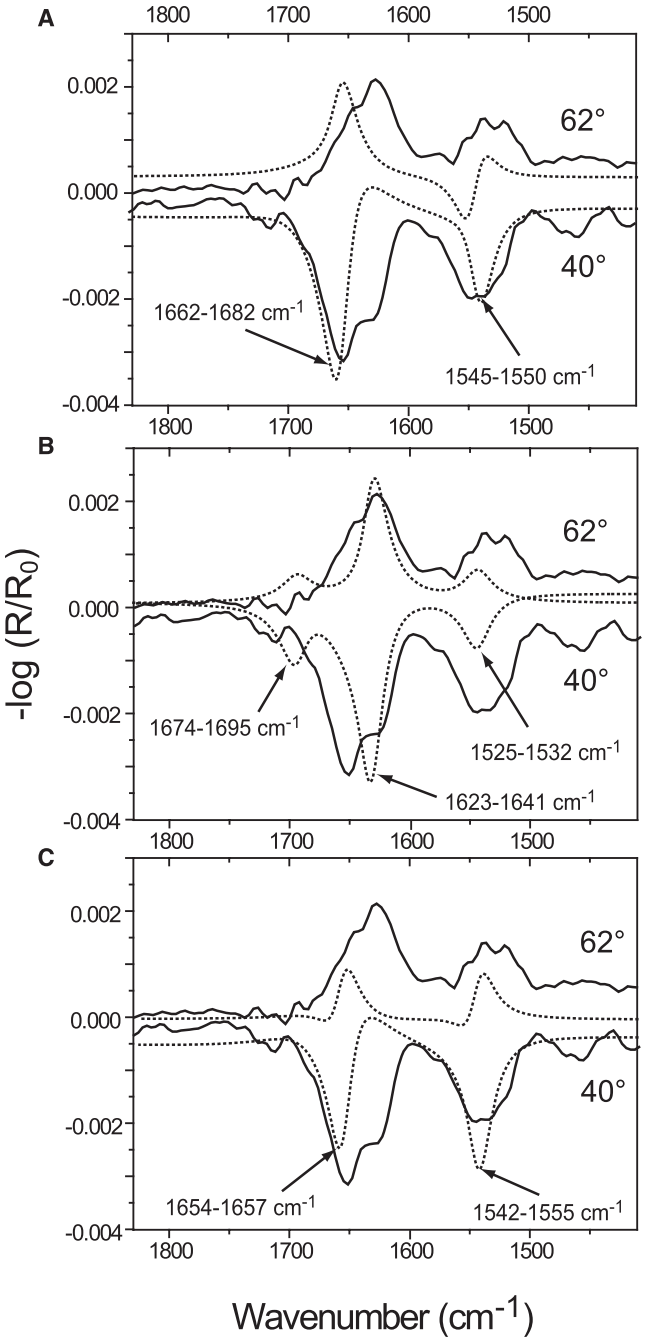

FIGURE 2 IRRA spectra of GST-PI3Kγ on Tris buffer at 9 mN/m acquired with p-polarized light at 40° and 62° (*solid lines*). Inserted are the corresponding simulated spectra (*dotted lines*) for (*A*) an α-helical structure lying flat at the interface, (*B*) a β-sheet lying flat at the air-buffer interface, and (*C*) a random coil structure. The spectra were calculated for an α-helix with a length of 1.5 nm and a width of 0.5 nm, and a β-sheet with a film thickness of 1 nm and the extinction coefficients of a model antiparallel β-sheet (47). The marked positions of the main bands are taken from Goormaghtigh et al.(48).

subphase. Strong van-der-Waals interactions between the long fatty-acid chains are the cause of the formation of densely packed condensed phases. The penetration into such a condensed lipid monolayer disturbs the chain packing, and this lack of energy cannot be compensated by other protein/lipid interactions. Even an electrostatically driven adsorption seems to be screened by small ions in the subphase. Therefore, the enzyme is not visible if the interface is covered with DSPC or DSPA monolayers.

The zwitterionic DMPC and the anionic DMPA have shorter symmetric fatty-acid chains. Therefore, they exhibited fluid phases at the pressures investigated. The dashed lines in Fig. 3 *B* represent DMPC and DMPA spectra in the amide band region at 5 mN/m without protein in the subphase. If protein is injected underneath these monolayers, the GST-PI3Kγ molecules penetrate into the lipid layer and the lateral pressure increases slightly. Amide bands of the protein are visible in the spectra of Fig. 3 *B* (*solid lines*), indicating enzyme adsorption/penetration. Compression of the mixed protein/lipid layer to 10 mN/m, i.e., slightly above the GST-PI3Kγ equilibrium pressure (9 mN/m), leads to a squeezing out of the protein, which desorbs into the bulk phase. The corresponding spectra in Fig. 3 *B* (*dotted lines*) are now similar to those recorded without protein in the subphase. At low surface pressure, the lipids DMPC and DMPA are loosely packed in the liquid-expanded phase, and therefore the interface provides enough space for occupation by protein molecules. The system becomes unstable when a critical pressure is reached. The lipids cannot stabilize the protein at the interface, demonstrating that no pronounced attractive interactions between the two components of the mixed layer are formed. The absence of strong attractive interactions might be caused by the nature of the used lipids, which are not substrates of this enzyme.

Finally, experiments with SAPC and SAPA were performed. In this case, the fatty-acid pattern is asymmetric. The glycerol backbone carries a stearoyl (18:0) fatty acid at the *sn*-1 position and an arachidonoyl (20:4) chain at the *sn*-2 position. These lipids exhibit only fluid monolayer phases. SAPC behaves similarly to the behavior of DMPC: The protein adsorbs/penetrates and is visible at the surface by IRRAS below the critical surface pressure only (data not shown). However, the experiments with SAPA show very different results (Fig. 3 *C*): The combination of unsaturation in the hydrophobic part and negative charge in the hydrophilic part of the lipid molecules provides conditions leading to a stabilization of the protein at the interface. The spectrum at 10 mN/m (data not shown) is almost the same as that observed at 5 mN/m (*solid line*), and it indicates that GST-PI3Kγ is not squeezed out above 9 mN/m. Moreover, the IRRA spectrum recorded at 30 mN/m (Fig. 3 *C*, *dotted line*) shows even increased intensities of the amide bands, indicating that the mixed layer can be compressed to quite high surface pressures. The increased intensity in the amide region is the result of either an increased concentration or a reorientation of the protein. The carbonyl band of the SAPA ester groups at ~1730 cm^{-1} cannot be detected after GST-PI3Kγ adsorption (Fig. 3*C*, *solid* and *dotted lines*). A reasonable explanation might be that a reorientation

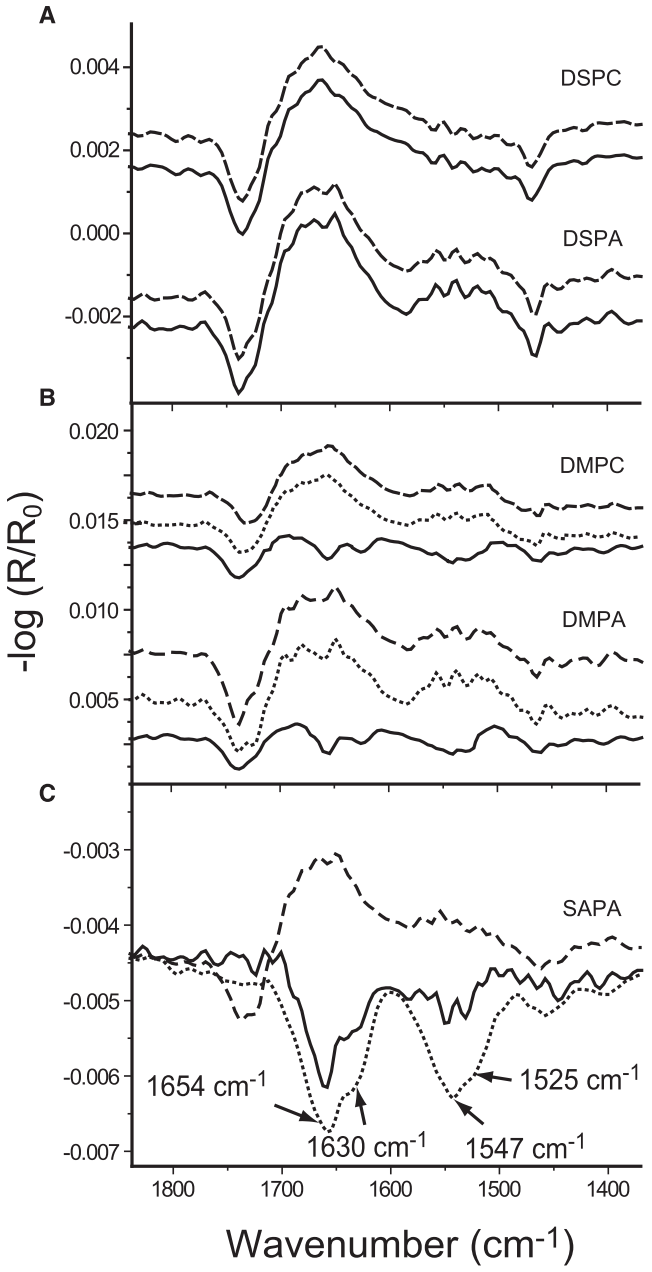

FIGURE 3 IRRA spectra of the Tris buffer surface with p-polarized light at 40° angle of incidence covered with (*A*) DSPC (*top*) and DSPA (*bottom*), with (*solid line*) and without (*dashed line*) GST-PI3Kγ at 5 mN/m; (*B*) DMPC (*top*) and DMPA (*bottom*), with GST-PI3Kγ at 5 mN/m (*solid line*), at 10 mN/m (*dotted line*), and without protein (*dashed line*). (*C*) SAPA with GST-PI3Kγ at 5 mN/m (*solid line*), at 30 mN/m (*dotted line*), and without GST-PI3Kγ (*dashed line*).

of the lipid molecules has taken place because of the interaction with the protein or a decrease of the absorption coefficient ε of the ν(CO) vibration of the lipidic ester carbonyl groups by protein-induced change of their chemical environment. This effect of the intensity decrease of the ester band can also be observed to a smaller extent with DMPA as well as with DMPC at 5 mN/m (Fig. 3 *B*, *solid line*). In this situation, the reduction of the lipid concentration in the footprint due to protein penetration is already a sufficient explanation, and reorientation of the lipid ester groups during protein adsorption and/or a smaller absorption coefficient do not necessarily need to be taken into account. Compression from 5 to 10 mN/m leads to the squeezing out of GST-PI3Kγ and the DMPA ester band recovers the intensity observed for the pure lipid monolayer (Fig. 3 *B*, *dotted* and *dashed lines*). To check whether the interaction with SAPA causes structural changes of the protein, IRRA spectra at different angles of incidence (40° and 62°) were recorded (data not shown). There is no significant change compared with the spectra observed with the pure protein at the bare air-buffer interface. However, the IRRA spectrum is very complex, and it is difficult to detect small changes in the secondary structure elements or their orientation.

Adsorption of GST-PI3Kγ at substrate monolayers

To prove whether substrate specificity of this enzyme has an additional/different influence on its adsorption behavior, a set of substrate phospholipids were used. The crucial difference between the results obtained with the nonsubstrate lipids and those obtained with the substrate lipids is that the protein was able to stay at the interface independent of the lipid phase state and of the surface pressure. This must be an effect of specific interactions of the protein with the inositol headgroups.

To examine the influence of the lipid headgroup structure on GST-PI3Kγ adsorption, unphosphorylated and phosphorylated inositols were investigated. The GST-PI3Kγ was injected into the subphase under the inositol monolayer, equilibrated at 5 mN/m. IRRA spectra of DPPtdIns (Fig. 4 *A*, *dotted line*) and DPPtdIns(4,5)P_2 (Fig. 4 *A*, *solid line*) monolayers were measured at 20 mN/m after compression. The protein adsorption is not enhanced by the higher charge density because of phosphorylation of the inositol headgroup. Indeed, very similar IRRA spectra have been obtained with GST-PI3Kγ in the presence of DPPtdIns(4,5)P_2 and DPPtdIns, except for the band at ~1625 cm^{-1}, which is largely decreased in the presence of DPPtdIns(4,5)P_2, in comparison to the results in the presence of DPPtdIns (Fig. 4 *A*). This indicates that the contribution of β-sheet structural elements in the amide I band of GST-PI3Kγ is smaller in the presence of DPPtdIns(4,5)P_2 than its contribution in the presence of DPPtdIns. The amide II signal of GST-PI3Kγ is also slightly decreased in the presence of DPPtdIns(4,5)P_2. One reason for these conditions could be a change of the orientation of the adsorbed GST-PI3Kγ caused by the presence of the phosphate groups. These results show that the high packing density in the condensed monolayers overcompensates for the attractive electrostatic interactions. Therefore, IRRA spectra were collected under the same conditions for fluid monolayers of DOPtdIns (Fig. 4 *B*, *dotted line*) and of DOPtdIns(4,5)P_2 (Fig. 4 *B*, *solid line*). The comparison of the amide band intensities

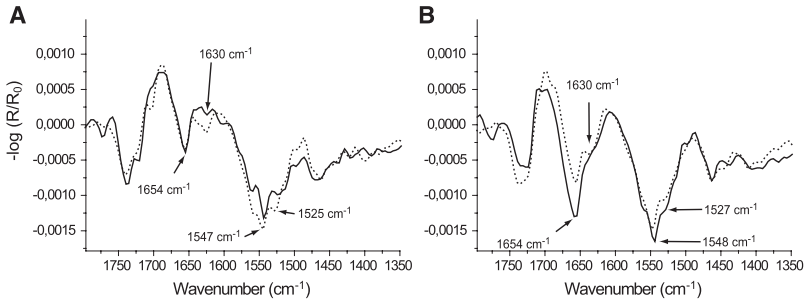

FIGURE 4 Influence of the headgroup structure on the GST-PI3Kγ affinity to PtdIns and PtdIns(4,5)P_2 monolayers. (*A*) IRRA spectra of DPPtdIns (*dotted line*) and DPPtdIns(4,5)P_2 (*solid line*) and (*B*) IRRA spectra of DOPtdIns (*dotted line*) and DOPtdIns(4,5)P_2 (*solid line*), with adsorbed GST-PI3Kγ on Tris buffer at 20 mN/m and acquired with p-polarized light at 40° angle of incidence. The kinase was injected at 5 mN/m. After protein adsorption, the film was compressed to 20 mN/m.

of adsorbed GST-PI3Kγ shows that, as long as the lipid packing allows protein adsorption and possibly penetration, the electrostatic interactions are enhanced by the stronger charged headgroups indicated by a significant increase of the intensity in the amide I region. The amide II/ amide I band ratio decreases, an effect that could be the result of a change in the orientation of the adsorbed GST-PI3Kγ, as explained above. Additionally, the effective protein layer thickness estimated from the intensity of the ν(OH) band at 3600 cm^{-1} is larger using phosphorylated DOPtdIns(4,5)P_2, compared with the results with DOPtdIns, whereas in the case of inositides with saturated chains, the number of phosphate groups has no influence on the intensity of this band (data not shown). Comparing the intensity of the amide bands in Fig. 4, *A* and *B*, the fluid unsaturated lipid appears clearly able to bind significantly more GST-PI3Kγ than the amount bound by the condensed saturated lipid. Therefore, one can conclude that the protein adsorption is driven primarily by electrostatic interactions, but higher lipid packing densities restrict the insertion into the monolayer.

To examine the influence of the fatty-acid pattern on the GST-PI3Kγ adsorption, IRRA spectra of bisphosphate inositols with different fatty-acid chains were compared after GST-PI3Kγ adsorption (Fig. 5). DPPtdIns(4,5)P_2 (Fig. 5, *dotted line*) has two equal saturated fatty-acid chains (C16:0). It exhibits an unusually broad phase coexistence region. The protein is able to interact with this lipid at surface pressures well above its equilibrium pressure. The protein signal is quite weak, but the bands in the amide region are clearly visible. The small intensity leads to the assumption that the protein concentration at the interface must be small. When the interface is covered with DOPtdIns(4,5)P_2, which carries two unsaturated oleoyl (C18:1) fatty acid chains, the protein shows a stronger adsorption (Fig. 5, *dashed line*). On compression, more adsorbed protein stays at/in the fluid monolayer compared with the the amount remaining at/in the more ordered layer of DPPtdIns(4,5)P_2. The shape of the amide bands is almost the same in both cases, indicating that the same protein structures are involved in the interaction with the two different lipids. As observed for the non-substrate phospholipids, a strongly enhanced interaction was observed for the asymmetrical 1-stearoyl-2-arachidonoyl (18:0,20:4) fatty-acid pattern present in SAPtdIns(4,5)P_2 (Fig. 5, *solid line*). The very pronounced amide I and II bands give evidence that the arachidonoyl chain in *sn*-2 position of the glycerol backbone provides optimal sterical conditions for the interaction with GST-PI3Kγ. This result is biologically significant, because naturally occurring lipids with the PtdIns(4,5)P_2 headgroup almost always have arachidonate in their *sn*-2 position, and most of them have stearate in their *sn*-1 position.

To prove whether there is indeed a specific interaction of GST-PI3Kγ adsorption with the fatty acids, IRRAS was used to monitor the phase state of the monolayer lipids. The symmetrical and asymmetrical stretching vibrations of the CH_2 groups are sensitive to conformational order and to the packing density of the hydrocarbon chains (33,34). For lipid chains in a liquid-expanded phase forming gauche conformers, the CH_2 stretching vibrations can be found at ~2924 cm^{-1} (asymmetric $\nu_{as}(CH_2)$) and ~2855 cm^{-1} (symmetric $\nu_s(CH_2)$). When the lipid chains are in the all-trans conformation (highly condensed phase), the corresponding stretching vibrations of the methylene groups are shifted to lower values and are located at ~2919 cm^{-1} for $\nu_{as}(CH_2)$ and ~2850 cm^{-1} for $\nu_s(CH_2)$. Fig. 6 *A* shows the $\nu_{as}(CH_2)$ positions as a function of surface pressure for DPPtdIns(4,5)P_2 monolayers on Tris buffer, and for DPPtdIns(4,5)P_2 monolayers on the same buffer containing GST-PI3Kγ. The transition region of DPPtdIns(4,5)P_2 on the Tris buffer is unusually broad. It can be seen that the

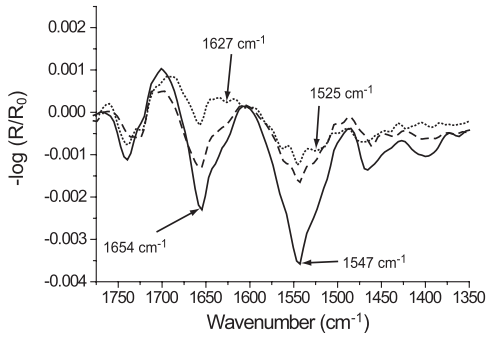

FIGURE 5 Influence of the fatty-acid pattern on GST-PI3Kγ affinity to PtdIns(4,5)P_2 monolayers. IRRA spectra of DP(16:0)- (*dotted line*), DO(18:1)- (*dashed line*), and stearoyl-arachidonoyl(18:0, 20:4)-PtdIns(4,5)P_2 (*solid line*) with adsorbed GST-PI3Kγ on Tris buffer at 20 mN/m and acquired with p-polarized light at 40° angle of incidence. The kinase was injected at 5 mN/m. After protein adsorption, the film was compressed to 20 mN/m.

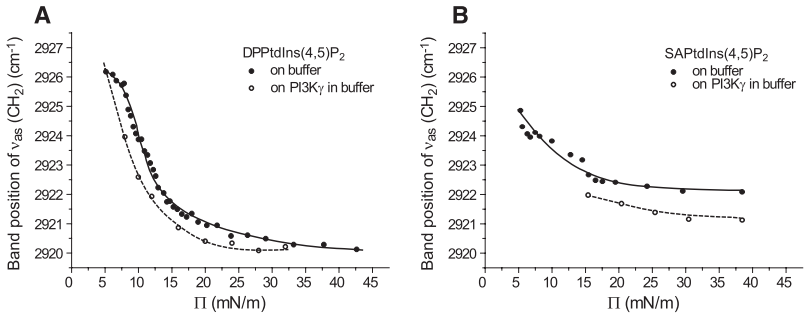

FIGURE 6 Band positions of the CH_2 asymmetrical stretching modes for (*A*) DPPtdIns(4,5)P_2 and (*B*) SAPtdIns(4,5)P_2 on Tris buffer as a function of surface pressure Π, with (*open circles, dashed lines*) and without (*closed circles, solid lines*) GST-PI3Kγ in the subphase. The corresponding spectra were acquired with p-polarized light at 40° angle of incidence.

phase behavior of this anionic phospholipid on compression is slightly influenced by GST-PI3Kγ. The interaction with the PtdIns(4,5)P_2 headgroup causes a small shift of the CH_2 bands toward lower wavenumbers at the same surface pressure. This can be interpreted as a small condensing effect of GST-PI3Kγ. The transition pressure taken at the midpoint of the transition range at 2923 cm^{-1} shifts from 11 to 9 mN/m. The lowest wavenumber of 2920 cm^{-1} is reached at 23 mN/m, at which point the protein is present, compared with the wavenumber at 33 mN/m on the pure buffer subphase, indicating a reduction of this broad transition range. At surface pressures above 33 mN/m, identical $\nu_{as}(CH_2)$ positions are found. The observed condensing effect indicates that the protein interacts preferentially with the disordered part of the monolayer.

Protein adsorption to SAPtdIns(4,5)P_2 monolayers on the same buffer and under the same experimental conditions leads immediately to a higher surface pressure of 15 mN/m. The protein again induces higher ordering and thus causes a tighter packing of the lipid molecules indicated by the lower wavenumber of the CH_2 band at the same surface pressure. The absolute value of this shift is similar to that observed with DPPtdIns(4,5)P_2 (approximately one wavenumber); however, the SAPtdIns(4,5)P_2 monolayer remains in the fluid state (Fig. 6 *B*). The intensities of all lipid bands with adsorbed GST-PI3Kγ are smaller compared with the intensity with pure lipid, because of the dilution of the lipid density in the footprint region by the penetrated protein.

IRRA spectra in the region of the phosphate stretching bands can provide information about the protonation state of the phosphate groups at the inositol. DPPtdIns(4,5)P_2 and SAPtdIns(4,5)P_2 were chosen to probe the response of the phosphate groups to protein adsorption. Changes in intensities and band positions can be seen in the phosphate region for both lipids after protein adsorption (Fig. 7, *A* and *B*). The phosphate-stretching-mode region is necessarily sensitive to the ionization state of the phosphate groups. Because of the subphase composition in the experiments, the phosphate groups are (at least partly) double ionized (35–37). The additional charge at the phosphate leads to a change of symmetry of this group (from meso- to isomorphic). Numerous bands are situated in the phosphate region (38,39). Therefore, the quantitative evaluation of the ionization state is difficult, and, thus, the evaluation will be discussed only qualitatively. The band observed at 1230 cm^{-1} in the spectra of the two phosphoinositides in Fig. 7 may be assigned to the asymmetric stretching mode of the single-charged species PO_2^-, by comparison with spectra of organophosphorus compounds and other phospholipids (39–42). The symmetric stretching mode of the double-charged species PO_3^{2-} arises at ~1000 cm^{-1}, in agreement with the findings of Klähn et al. (43) and Laroche et al. (44), who found comparable results for phosphates in aqueous solutions or in DMPA. The most intense band at 1090 cm^{-1} can be either assigned to the symmetric stretching mode of PO_2^- or to the asymmetric one of PO_3^{2-} (43).

The shift of the asymmetrical phosphate band at 1230 cm^{-1} to slightly lower wavenumbers, compared with phosphate-band shifts of other anionic phospholipids (31), indicates strong hydration and a possible involvement in hydrogen bonding. The influence of water for stabilizing PtdIns(4,5)P_2 monolayers seems to be evident. The phosphates carried by the inositol headgroup are double charged in the physiologic buffer, because a symmetric stretching

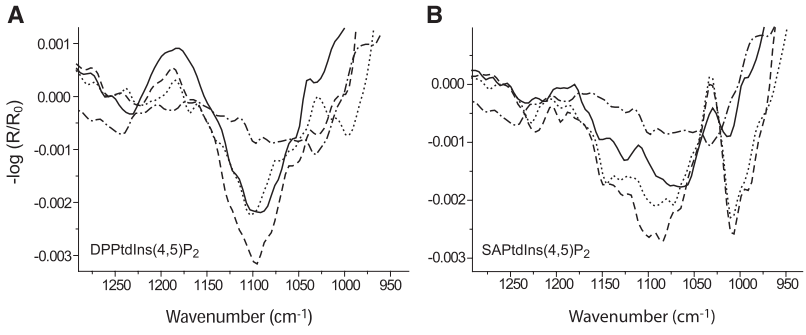

FIGURE 7 Phosphate band region of IRRA spectra of DPPtdIns(4,5)P_2 and SAPtdIns(4,5)P_2 on Tris buffer with and without GST-PI3Kγ . (*A*) DPPtdIns(4,5)P_2 with protein at 15 mN/m (*solid line*) and without protein at 15 mN/m (*dotted line*) and at 30 mN/m (*dashed line*). (*B*) SAPtdIns(4,5)P_2 with protein at 15 mN/m (*solid line*) and without protein at 15 mN/m (*dotted line*) and at 30 mN/m (*dashed line*). Spectra were collected with p-polarized light at 40° angle of incidence. The kinase was injected at 5 mN/m. After protein adsorption, the film was compressed to the corresponding surface pressures. The spectra (*dotted-dashed line*) observed with the pure protein (Fig. 1) have been added for comparison.

band for PO_3^{2-} at ~1000 cm^{-1} can be observed in most IRRA spectra (Fig. 7). This band was much more intense in the case of SAPtdIns(4,5)P_2 (Fig. 7 *B*), compared with the intensity with DPPtdIns(4,5)P_2 (Fig. 7 *A*), because the condensed state of the latter phosphoinositol prevented high-charge densities. The packing-mode-dependent ionization was recently demonstrated by Antipina et al. (45) for cationic phospholipids and has to be taken into account concerning the data interpretation. In the case of DPPtdIns(4,5)P_2, the intensity of the band at ~1000 cm^{-1} decreased upon compression from 15 to 30 mN/m, indicating a decrease of the amount of the double charged phosphates due to higher packing density (Fig. 7 *A*, *dotted* and *dashed lines*). The band vanished almost completely upon GST-PI3Kγ adsorption at 15 mN/m (Fig. 7 *A*, *solid line*), whereas the intensity at ~1230 cm^{-1} remained the same or increased even slightly, indicating that PO_2^- is stabilized compared to PO_3^{2-} by the presence of the protein. In the case of SAPtdIns(4,5)P_2, however, the intensity of the prominent band at ~1000 cm^{-1} decreased to about one third of its original value. This result can be explained in the same way as in the case of DPPtdIns(4,5)P_2, keeping in mind that the ionization state of the phosphate groups of SAPtdIns(4,5)P_2 was much higher from the beginning because of the liquid-expanded state. Additionally, the intensity at ~1230 cm^{-1} decreased significantly upon protein adsorption. This observation supports the assumption that, in contrast to condensed DPPtdIns(4,5)P_2, the single-charged phosphate groups at the *sn*-3 position of the glycerol backbone are also accessible for the protein leading to the protonation of some of these groups by a pK change.

The strength of GST-PI3Kγ interactions with the negatively charged headgroups is clearly influenced by the phase state of the lipid monolayer. Concerning the two substrate inositol phospholipids, the decrease of the PO_3^{2-} stretching modes was observed for both the condensed and fluid-expanded phases. When the protein was adsorbed, the symmetrical PO_3^{2-} stretching band was only weak or absent. One reason for this observation could be a reorientation of the phosphate induced by the GST-PI3Kγ adsorption. Another interpretation, that a protein-induced protonation of the phosphate groups occurred, is more favorable, because the charge-stabilizing hydrogen bonding is disturbed by the protein adsorption. Subsequently, strong repulsive forces between the headgroups emanate. It was recently shown for myo-inositol phosphates that, depending on the ionic environment, the pK values of the phosphate groups will shift (46). If we expect a perturbation of the (shielding) water between and below the headgroups, the ions have better access to the charges and change the local pH at the interface. Subsequently, the phosphate groups become protonated.

CONCLUSIONS

With the help of infrared reflection-absorption spectroscopy, important structural requirements for the GST-PI3Kγ adsorption have been identified. Adsorbed at the air-buffer interface, the protein has an equilibrium pressure of ~9 mN/m and shows a great variety of secondary structure elements, including β-sheets. GST-PI3Kγ does not adsorb at condensed zwitterionic or anionic monolayers, and it is squeezed out from fluid zwitterionic or anionic monolayers on compression. Only in the case of SAPA (negatively charged, fluid, and with the arachidonoyl chain in *sn*-2 position), GST-PI3Kγ adsorbs, penetrates, and remains in the monolayer even at pressures well above the equilibrium pressure. The same has been observed with substrate phospholipids on a much higher level. Using condensed phosphoinositide monolayers, the bands appearing during GST-PI3Kγ adsorption are comparably weak. In agreement with the results observed for nonsubstrate lipids, the highest protein affinity was observed for a fatty-acid pattern with the arachidonoyl chain in *sn*-2 position. The protein does not change its structure significantly upon lipid binding, but it has a strong influence on the lipid layer. GST-PI3Kγ adsorption condenses the phospholipid monolayers. This effect is again strongest for the unsaturated lipids (due to the stronger protein adsorption). Furthermore, the GST-PI3Kγ interaction with the substrate molecules promotes the protonation of their phosphate groups, thereby reducing the charge density of the lipid monolayer. This effect is stronger for the fluid-expanded SAPtdIns(4,5)P_2 monolayer, compared to the effect for the condensed DPPtdIns(4,5)P_2 monolayer, because less phosphate groups are double deprotonated because of the higher packing density in the condensed layer. The effect of the packing density can be understood in the following way: the smaller the distance between the charged phosphate groups, the stronger their electrostatic repulsion and the higher the pK. Nevertheless, the protonation process is observable in both cases, indicating that the phosphate groups attached to the inositol headgroup, rather than the phosphoester link to the glycerol backbone, are involved. That effect is most likely caused by the disturbance of the hydrogen bonding network between the headgroups, which stabilizes the charges at the interface respectively and assists their deprotonation. The protein affinity to the monolayer/buffer interface can be enhanced by increasing the charge density. Therefore, a larger amount of adsorbed GST-PI3Kγ was observed using the PtdIns(4,5)P_2, compared to the amount for inositide isoform with no phosphate groups attached to the headgroup.

To sum up, GST-PI3Kγ interacts directly with phospholipids. This interaction, which is mainly electrostatically driven and stabilized by hydrophobic forces, changes the physical-chemical properties of the inner leaflet of the membrane. In particular, the combination of phosphorylation of the inositol and the specific stearoyl-arachidonoyl fatty-acid pattern enhances the interactions between the protein and the lipid drastically. GST-PI3Kγ stays attached to the surface well above its equilibrium surface pressure, and the protein strongly influences the lipid headgroups in terms of ionization and conformation.

The authors thank Arne Gericke and Richard Mendelsohn for fruitful discussions and Annabel Muenter for technical coaching of the use of the IRRAS instrument.

REFERENCES

1. Martin, T. F. J. 1998. Phosphoinositide lipids as signaling molecules: common themes for signal transduction, cytoskeletal regulation, and membrane trafficking. *Annu. Rev. Cell Dev. Biol.* 14:231–264.
2. Rameh, L. E., and L. C. Cantley. 1999. The role of phosphoinositide 3-kinase lipid products in cell function. *J. Biol. Chem.* 274:8347–8350.
3. Toker, A. 2002. Phosphoinositides and signal transduction. *Cell. Mol. Life Sci.* 59:761–779.
4. Vanhaesebroeck, B., K. Higashi, C. Raven, M. Welham, S. Anderson, et al. 1999. Autophosphorylation of p110δ phosphoinositide 3-kinase: a new paradigm for the regulation of lipid kinases in vitro and in vivo. *EMBO J.* 18:1292–1302.
5. Vanhaesebroeck, B., G. E. Jones, W. E. Allen, D. Zicha, R. Hooshmand-Rad, et al. 1999. Distinct PI(3)Ks mediate mitogenic signalling and cell migration in macrophages. *Nat. Cell Biol.* 1:69–71.
6. Vanhaesebroeck, B., and M. D. Waterfield. 1999. Signaling by distinct classes of phosphoinositide 3-kinases. *Exp. Cell Res.* 253:239–254.
7. Wymann, M. P., and L. Pirola. 1998. Structure and function of phosphoinositide 3-kinases. *Biochim. Biophys. Acta.* 1436:127–150.
8. Stephens, L., A. Smrcka, F. T. Cooke, T. R. Jackson, P. C. Sternweis, et al. 1994. A novel phosphoinositide 3 kinase activity in myeloid-derived cells is activated by G protein $\beta\gamma$ subunits. *Cell.* 77:83–93.
9. Ma, A. D., A. Metjian, S. Bagrodia, S. Taylor, and C. S. Abrams. 1998. Cytoskeletal reorganization by G protein-coupled receptors is dependent on phosphoinositide 3-kinase γ, a Rac guanosine exchange factor, and Rac. *Mol. Cell Biol.* 18:4744–4751.
10. Murga, C., L. Laguinge, R. Wetzker, A. Cuadrado, and J. S. Gutkind. 1998. Activation of Akt/protein kinase B by G protein-coupled receptors. A role for α and $\beta\gamma$ subunits of heterotrimeric G proteins acting through phosphatidylinositol-3-OH kinase γ. *J. Biol. Chem.* 273: 19080–19085.
11. Stoyanova, S., G. Bulgarelli-Leva, C. Kirsch, T. Hanck, R. Klinger, et al. 1997. Lipid kinase and protein kinase activities of G-protein-coupled phosphoinositide 3-kinase γ: structure-activity analysis and interactions with wortmannin. *Biochem. J.* 324:489–495.
12. Perrino, C., S. V. N. Prasad, J. N. Schroder, J. A. Hata, C. Milano, et al. 2005. Restoration of β-adrenergic receptor signaling and contractile function in heart failure by disruption of the βARK1/phosphoinositide 3-kinase complex. *Circulation.* 111:2579–2587.
13. Patrucco, E., A. Notte, L. Barberis, G. Selvetella, A. Maffei, et al. 2004. PI3Kγ modulates the cardiac response to chronic pressure overload by distinct kinase-dependent and -independent effects. *Cell.* 118: 375–387.
14. Kirsch, C., R. Wetzker, and R. Klinger. 2001. Anionic phospholipids are involved in membrane targeting of PI 3-kinase γ. *Biochem. Biophys. Res. Commun.* 282:691–696.
15. Hirsch, E., V. L. Katanaev, C. Garlanda, O. Azzolino, L. Pirola, et al. 2000. Central role for G protein-coupled phosphoinositide 3-kinase γ in inflammation. *Science.* 287:1049–1053.
16. Sasaki, T., J. Irie-Sasaki, R. G. Jones, A. J. Oliveira-dos-Santos, W. L. Stanford, et al. 2000. Function of PI3Kγ in thymocyte development, T cell activation, and neutrophil migration. *Science.* 287:1040–1046.
17. Suire, S., W. J. Coadwell, G. J. Ferguson, K. Davidson, P. T. Hawkins, et al. 2005. P84, a new G$\beta\gamma$-activated regulatory subunit of the type IB phosphoinositide 3-kinase p110γ. *Curr. Biol.* 15:566–570.
18. Brock, C., M. Schaefer, H. P. Reusch, C. Czupalla, M. Michalke, et al. 2003. Roles of G$\beta\gamma$ in membrane recruitment and activation of p110γ/p101 phosphoinositide 3-kinase γ. *J. Cell Biol.* 160:89–99.
19. Feng, S. S. 1999. Interpretation of mechanochemical properties of lipid bilayer vesicles from the equation of state or pressure-area measurement of the monolayer at the air-water or oil-water interface. *Langmuir.* 15:998–1010.
20. Dluhy, R. A. 1986. Quantitative external reflection infrared spectroscopic analysis of insoluble monolayers spread at the air-water interface. *J. Phys. Chem.* 90:1373–1379.
21. Dluhy, R. A., and D. G. Cornell. 1985. *In situ* measurement of the infrared spectra of insoluble monolayers at the air-water interface. *J. Phys. Chem.* 89:3195–3197.
22. Dluhy, R. A., M. L. Mitchell, T. Pettenski, and J. Beers. 1988. Design and interfacing of an automated Langmuir-type film balance to an FT-IR Spectrometer. *Appl. Spectrosc.* 42:1289–1293.
23. Mendelsohn, R., J. W. Brauner, and A. Gericke. 1995. External infrared reflection absorption spectrometry of monolayer films at the air-water interface. *Annu. Rev. Phys. Chem.* 46:305–334.
24. Cabiaux, V., B. Agerberth, J. Johansson, F. Homble, E. Goormaghtigh, et al. 1994. Secondary structure and membrane interaction of PR-39, a Pro+Arg-rich antibacterial peptide. *Eur. J. Biochem.* 224:1019–1027.
25. Cai, P., C. R. Flach, and R. Mendelsohn. 2003. An infrared reflection-absorption spectroscopy study of the secondary structure in $(KL_4)_4K$, a therapeutic agent for respiratory distress syndrome, in aqueous monolayers with phospholipids. *Biochemistry.* 42:9446–9452.
26. Zhou, Y., L. Fang, D. Du, W. Zhou, X. Feng, et al. 2008. Proteome identification of binding-partners interacting with cell polarity protein Par3 in Jurkat cells. *Acta Biochim. Biophys. Sin. (Shanghai).* 40:729–739.
27. Phi, Q. T., Y. M. Park, C. M. Ryu, S. H. Park, and S. Y. Ghim. 2008. Functional identification and expression of indole-3-pyruvate decarboxylase from *Paenibacillus polymyxa* E681. *J. Microbiol. Biotechnol.* 18:1235–1244.
28. Tan, F., L. Lu, Y. Cai, J. Wang, Y. Xie, et al. 2008. Proteomic analysis of ubiquitinated proteins in normal hepatocyte cell line Chang liver cells. *Proteomics.* 8:2885–2896.
29. Trudel, E., S. Beaufils, A. Renault, R. Breton, and C. Salesse. 2006. Binding of RPE65 fragments to lipid monolayers and identification of its partners by glutathione *S*Transferase pull-down assays. *Biochemistry.* 45:3337–3347.
30. Walker, E. H., O. Perisic, C. Ried, L. Stephens, and R. L. Williams. 1999. Structural insights into phosphoinositide 3-kinase catalysis and signalling. *Nature.* 402:313–320.
31. Maltseva, E., A. Kerth, A. Blume, H. Möhwald, and G. Brezesinski. 2005. Adsorption of amyloid β (1–40) peptide at phospholipid monolayers. *Chem. Bio. Chem.* 6:1817–1824.
32. Chirgadze, Y. N., and N. A. Nevskaya. 1976. Infrared spectra and resonance interaction of amide-I vibration of the antiparallel-chain pleated sheet. *Biopolymers.* 15:607–625.
33. Macphail, R. A., H. L. Strauss, R. G. Snyder, and C. A. Elliger. 1984. C-H stretching modes and the structure of *n*-alkyl chains. 2. Long, all-trans chains. *J. Phys. Chem.* 88:334–341.
34. Snyder, R. G., H. L. Strauss, and C. A. Elliger. 1982. C-H stretching modes and the structure of *n*-alkyl chains. 1. Long, disordered chains. *J. Phys. Chem.* 86:5145–5150.
35. Galla, H. J., and E. Sackmann. 1975. Chemically induced lipid phase separation in model membranes containing charged lipids: a spin label study. *Biochim. Biophys. Acta.* 401:509–529.
36. Galla, H. J., and E. Sackmann. 1975. Chemically induced phase separation in mixed vesicles containing phosphatidic acid. An Optical Study. *J. Am. Chem. Soc.* 97:4114–4120.
37. Träuble, H., and H. Eibl. 1974. Electrostatic effects on lipid phase transitions: membrane structure and ionic environment. *Proc. Natl. Acad. Sci. USA.* 71:214–219.
38. Tamm, L. K., and S. A. Tatulian. 1997. Infrared spectroscopy of proteins and peptides in lipid bilayers. *Q. Rev. Biophys.* 30:365–429.
39. Thomas, L. C., and R. A. Chittenden. 1970. Characteristic infrared absorption frequencies of organophosphorus compounds-VII. Phosphorus ions. *Spectrochim. Acta. [A].* 26:781–800.

40. Casal, H. L., U. Kohler, H. H. Mantsch, F. M. Goni, and J. L. R. Arrondo. 1987. Conformational changes in proteins induced by low-temperatures: an infrared study. *Z. Naturforsch. [C]*. 42:1339–1342.

41. Casal, H. L., H. H. Mantsch, F. Paltauf, and H. Hauser. 1987. Infrared and 31P-NMR studies of the effect of Li^+ and Ca^{2+} on phosphatidylserines. *Biochim. Biophys. Acta*. 919:275–286.

42. Casal, H. L., A. Martin, H. H. Mantsch, F. Paltauf, and H. Hauser. 1987. Infrared studies of fully hydrated unsaturated phosphatidylserine bilayers. Effect of Li^+ and Ca^{2+}. *Biochemistry*. 26:7395–7401.

43. Klähn, M., G. Mathias, C. Kötting, M. Nonella, J. Schlitter, et al. 2004. IR Spectra of phosphate ions in aqueous solution: predictions of a DFT/MM approach compared with observations. *J. Phys. Chem. A*. 108:6186–6194.

44. Laroche, G., E. J. Dufourc, J. Dufourcq, and M. Pezolet. 1991. Structure and dynamics of dimyristoylphosphatidic acid/calcium complexes by 2H NMR, infrared, and Raman spectroscopies and small-angle X-ray diffraction. *Biochemistry*. 30:3105–3114.

45. Antipina, M. N., B. Dobner, O. V. Konovalov, V. L. Shapovalov, and G. Brezesinski. 2007. Investigation of the protonation state of novel cationic lipids designed for gene transfection. *J. Phys. Chem. B*. 111:13845–13850.

46. Yang, P., B. Spiess, P. N. M. Pushpalatha, and R. E. Brown. 2007. Influence of metal cations on the intramolecular hydrogen-bonding network and pK_a in phosphorylated compounds. *J. Phys. Chem. A*. 111:3602–3612.

47. Buffeteau, T., E. Le Calvez, S. Castano, B. Desbat, D. Blaudez, et al. 2000. Anisotropic optical constants of α-helix and β-sheet secondary structures in the infrared. *J. Phys. Chem. B*. 104:4537–4544.

48. Goormaghtigh, E., V. Cabiaux, and J.-M. Ruysschaert. 1994. Determination of soluble and membrane protein structure by Fourier transform infrared spectroscopy. III. Secondary Structures. *In* Physicochemical Methods in the Study of Biomembranes. H.J. Hilderson and G.B. Ralston, editors. *In* Subcellular Biochemistry, Vol. 23. Plenum Press, New York. 405–450.